Controlling Kink Band Morphology in Block Copolymers: Threshold Criteria and Stability

Daniel L. Polis and Karen I. Winey*

Laboratory for Research on the Structure of Matter, Department of Materials Science and Engineering, University of Pennsylvania, Philadelphia, Pennsylvania 19104-6272

Received December 19, 1997; Revised Manuscript Received March 2, 1998

ABSTRACT: The initiation, structure, and dynamics of defects control both the structure and physical properties of materials. In this work, kink band defects are systematically introduced into a lamellar poly(styrene-*b*-ethylene propylene) diblock copolymer by applying various rates and total strains of steady shear. However, kink bands are only produced when the shear strain exceeds a critical value. The mere existence of kink bands implies the presence of a preferential slip plane parallel to the lamellae, which we estimate exists within the polystyrene microdomains. Furthermore, our results regarding the dependence of kink band geometry on shear rate and strain suggest that these defects are formed by the rotation of lamellae. Based on a rotation mechanism, the characteristic size of the kink bands and their spatial distribution, it appears that preexisting defects initiate kink bands. Insights gained from steady-shear-induced kink bands are extended to oscillatory shear alignment of this high molecular weight diblock copolymer, allowing us to circumvent a previously reported shear-stabilized parallel-transverse biaxial texture.

Introduction

Kink bands have long been observed in crystalline solids, minerals, foliated rocks, and model systems when subjected to mechanical deformation.[1−3] Kink bands are tabular zones of sheared material in which the slip plane or foliation is rotated relative to the matrix material. A natural kink band in laminated siltstone separated by clay-rich layers is shown in Figure 1a.[4] Each layer transversing the kink band has two angular or sharp folds of opposite sense. These folds or hinges separate a short limb from longer limbs on either side of the kink band. The repetition of these angular folds through neighboring layers constitutes a kink band. The two rows of angular folds correspond to the boundaries of the kink band. Although the geometry of kink bands is universal, their size varies widely (as does the periodicity of the layers) from submicron widths for crystalline solids to widths of as much as several meters for sedimentary rocks.

We report here the first forward kink bands in a lamellar diblock copolymer. Although the layer periodicity between foliated rocks and block copolymers varies by more than 4 orders of magnitude, we demonstrate that the formation and morphologies of kink bands are analogous. Structural geologists have shown that detailed studies of multilayer folding can elucidate materials properties and deformation mechanisms. Similarly, studies of kink bands and other layer folding phenomena, such as chevron folding,[5,6] provide insight into the dynamics and alignment of block copolymers. For example, the formation of kink bands indicates the presence of a preferential slip plane parallel to the lamellar microdomains in a block copolymer. Furthermore, kink band formation suggests that the microphase separated domains remain intact and rotate during mechanical deformation. Although many researchers have studied shear-induced alignment in block copolymers,[7−9] important issues remain unresolved, such as: the mechanisms of shear-induced alignment, the importance of viscoelastic contrast between blocks, and the significance of defect-mediated rheology. Systematic studies of kink bands and other defects could elucidate these key questions.

In addition to providing insight into block copolymer dynamics, defects can be used to control morphology and thereby the physical properties. Csernica and coworkers[10] showed that the gas permeability varies depending on lamellar orientation and alignment in a poly(styrene-*b*-butadiene) diblock copolymer. Therefore, avoiding kink bands may be important in order to optimize the properties of interest. In contrast, controlling kink band size, density, and orientation may provide additional control over physical properties. In this report, we apply our results regarding steady-shear-induced kink band formation to large amplitude oscillatory shear alignment to obtain contrasting morphologies.

Experimental Section

Material. The lamellar poly(styrene-*b*-ethylene propylene) diblock copolymer studied was Kraton G1701 provided by Shell Chemical Company. As previously reported, this diblock copolymer has a weight average molecular weight of 110 000 g/mol, a polydispersity index of 1.03, and a styrene monomeric unit content of 37 wt %.[11] The material is therefore referred to as SEP(40−70), corresponding to the nominal average M_ws of the polystyrene (PS) and poly(ethylene propylene) (PEP) blocks. The microphase separation transition temperature (MST) was not observed upon heating to ∼300 °C and has been estimated to be >300 °C, making it experimentally inaccessible. The SEP(40−70) samples were produced by solvent casting followed by compression molding.[11]

Rheology. A Rheometrics solids analyzer (RSAII), with shear sandwich geometry, was used to apply both large amplitude oscillatory shear (LAOS) and steady shear to SEP(40−70) specimens. First, LAOS was used to create a primarily parallel starting state using a strain amplitude, frequency and temperature of 20%, 0.5 rad/s, and 180 °C, respectively. This temperature is above the glass transition temperature of the PS block (102 °C) and well below the MST of SEP(40−70). After 1 h of LAOS, samples were quiescently annealed in the rheometer at 180 °C for 2 h. Following this initial alignment, steady shear was applied at a fixed rate (0.005,

S0024-9297(97)01839-1 CCC: $15.00
Published on Web 05/13/1998

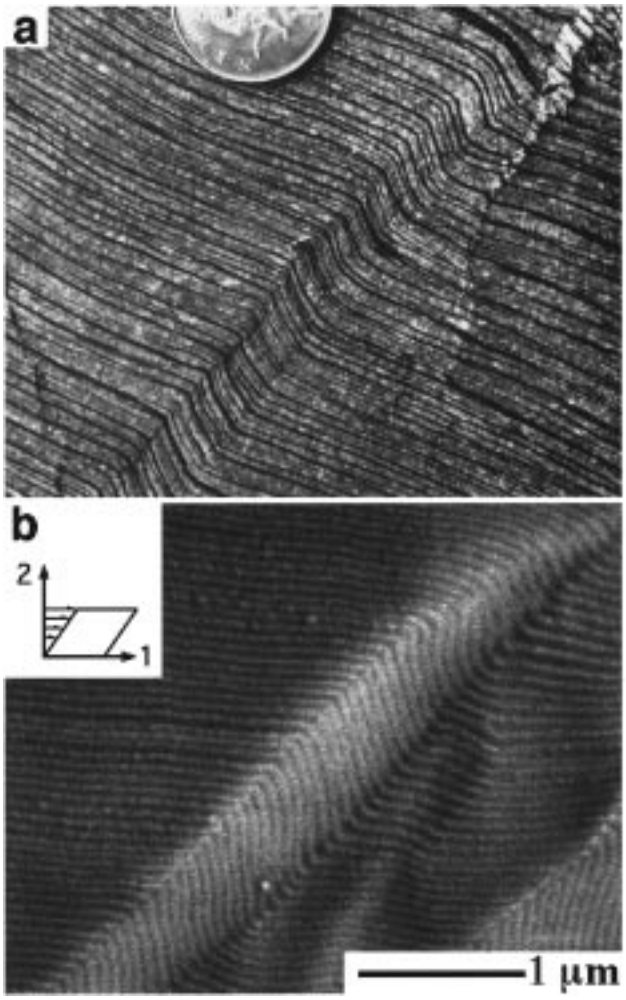

Figure 1. (a) A kink band in a laminated rock of siltstone and clay-rich layers (scale indicated by coin), reproduced from ref 4. (b) FE-SEM micrograph showing a representative kink band in SEP(40−70) following steady shear (180 °C, 0.05 s^{-1}, 80% strain). The inset illustrates the orientation of the steady shear relative to the image plane. The contrast in this secondary electron image is the result of staining the PS lamellae with RuO_4, so that they appear brighter than the PEP lamellae. Both examples illustrate the characteristic kink band geometry: two rows of angular hinges separating one short limb from longer limbs on either side.

0.05, or 0.1 s^{-1}) for total strains ranging from 20 to 80%. The samples were quenched (cooled to room temperature in <1 min) immediately following this steady shear deformation and removed for morphological evaluation. Rapid quenching is necessary to avoid changes in lamellar orientation and boundary curvature, which occur during quiescent annealing.[12] In a separate experiment, field emission-scanning electron microscopy (FE-SEM) and small-angle x-ray scattering (SAXS) were used to confirm the parallel orientation of the starting state. Specifically, following the alignment procedure (1 h LAOS and 2 h anneal), a sample was quenched and removed from the rheometer for morphological evaluation.

FE-SEM. Blocks were cut to ∼5 × 5 mm and mounted on specimen stubs with the neutral direction oriented perpendicular to the stub surface. The velocity, velocity-gradient, and neutral directions will be referred to as the 1, 2, and 3 directions, respectively. The 3 direction provides the most convenient view of the kink bands for reasons described in our previous work.[12] The samples were then prepared for microscopy using a cryoultramicrotome (Reichert Ultracut S) operated at −80 °C, which is below the glass transition temperature of the PEP block. A small mesa, ∼ 0.5 × 0.5 mm, was formed on each specimen with a glass knife. A glass knife was also used to microtome 90-nm sections from the top of the mesa, creating a smoother block face.

Polystyrene latex nanospheres from Polysciences Inc. (Warrington, PA) served as calibrants for the microscope magnification and aided in focusing on the flat samples. These spheres, 503 nm in diameter, were distributed on the samples with an aspirator to prevent them from clustering on the surface. Samples were then stained for ∼30 min by the vapors of an aqueous solution of 5% RuO_4, which preferentially stains the styrene monomeric units. A coating of Cr, ∼ 2 nm thick, was evaporated on the samples to reduce charging during scanning electron microscopy.

To maximize resolution and minimize charging and sample degradation, the microscopy was performed on a scanning electron microscope equipped with a field emission electron gun (FE-SEM), specifically the JEOL 6300 FV. The FE-SEM was operated between 1.0 and 2.0 kV. Some samples were tilted to increase the electron collection efficiency, however, corrections were made to account for any sample tilt when analyzing images. Secondary electron images were acquired digitally from a sample using JEOL's Vision software. The images were transferred to a Macintosh 7100 where Adobe Photoshop 3.04 was used to adjust the contrast and brightness. Image analysis was done with NIH Image 1.61.

SAXS. SAXS was performed using a reconditioned and upgraded Elliot GX-6 rotating anode (Cu Kα) operated at 40 kV with a 0.2 × 2-mm microfocus cathode, pinhole optics, and Ni foil monochromation. A Siemens HI−STAR area detector was used at the end of a 110-cm He-filled flight path. A stained collagen sample from a duck's tendon, which has a repeat distance of 609 Å, was used for angular calibration of the detector. Scattering experiments were performed with the beam oriented parallel to the 1, 2, and 3 directions to determine the degree of alignment in SEP(40−70) specimens following various LAOS conditions. The parasitic scattering was subtracted from the SAXS data. The SAXS results following steady shear deformations are not discussed because they did not indicate any significant morphological changes from our starting state. The SAXS did not detect the shear-induced kink bands because they are small in size and number density, unlike the conjugate kink bands responsible for the four-spot SAXS patterns reported by Pinheiro et al.[11,12]

Results

To simplify the analysis of kink band formation, kink bands were produced in specimens having a predominately parallel initial orientation. This is in contrast to our previous work,[11,12] in which a biaxial texture, corresponding to conjugate kink bands, was produced from an initially unaligned sample. The predominately parallel starting state was produced by applying LAOS and annealing for 2 h, as already described. SAXS confirmed this primarily parallel orientation. The degree of alignment is most clearly illustrated through an examination of the scattered intensity as a function of azimuthal angle, μ. Figure 2 shows the integrated scattered intensity of the fourth-order Bragg peak, $I_4(\mu)$, as a function of μ with the beam oriented parallel to the 1*, 2*, and 3* directions. Here, the 1*, 2*, and 3* refer to reciprocal space directions that are parallel to the real space directions (velocity, velocity-gradient, and neutral, respectively) in this orthogonal coordinate system. The scattering volume was approximately equal for the three scattering experiments in Figure 2 and thus the intensity was not normalized. A maximum exists along the 2* direction that is evident when the beam is parallel to either the 1* or 3* direction, and corresponds to scattering from lamellae in the parallel orientation. The breadth of these peaks indicates the presence of lamellae that are slightly misaligned relative to the parallel orientation. An SEM micrograph of

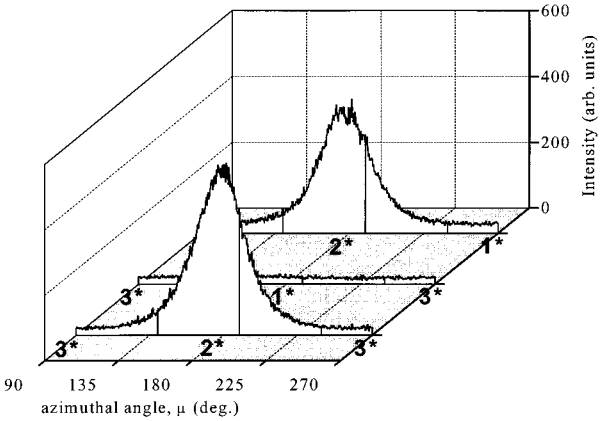

Figure 2. $I_4(\mu)$ as a function of μ for a SEP(40−70) specimen that was aligned as described in the *Experimental Section*. The three intensity distributions correspond to SAXS experiments in which the beam was orientated parallel to the 1*, 2*, and 3* directions. The predominately parallel alignment is apparent from the intensity maxima observed along the 2* direction. Furthermore, the weak but uniform scattering intensity observed when the beam is parallel to the 2* direction indicates that there is no preference for either the transverse or perpendicular lamellar orientation, which scatter along the 1* and 3* directions, respectively.

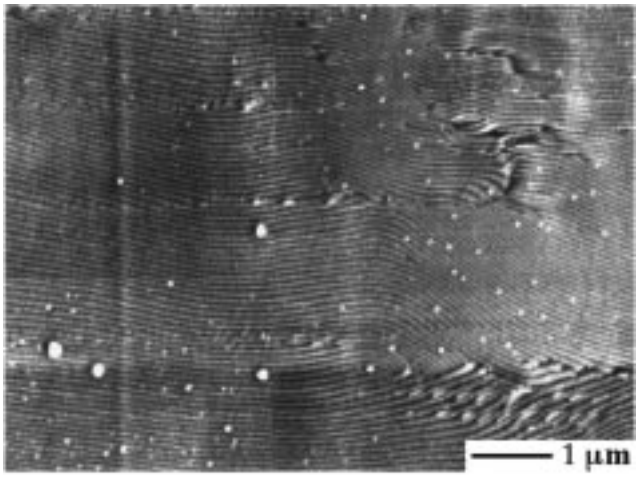

Figure 3. FE-SEM micrograph showing a SEP(40−70) specimen following the alignment procedure described in the *Experimental Section*. The lamellae have normals oriented parallel or nearly parallel to the 2 direction. This result is consistent with the SAXS results, indicating a predominately parallel orientation. However, some remaining defects are present in this predominately parallel starting state. The LAOS was oriented as that of the steady shear shown in the inset of Figure 1b.

SEP(40−70) quenched following the alignment procedure is shown in Figure 3. Along with slightly misaligned lamellae, this micrograph shows a primarily parallel orientation. Thus, from both the SAXS intensity distribution and SEM it is evident that we have produced a predominately parallel orientation. Note that SEM revealed a kink-band-free morphology, indicating that these LAOS conditions (20%, 0.5 rad/s, 180 °C, 1 h) are not sufficient to produce kink bands in an unaligned specimen. Furthermore, application of LAOS (20%, 0.5 rad/s, and 180 °C as before) for 6 h produced a similar degree of parallel alignment from an initially unaligned SEP(40−70) specimen.

Steady shear applied to SEP(40−70) in a predominately parallel orientation produces forward kink bands.

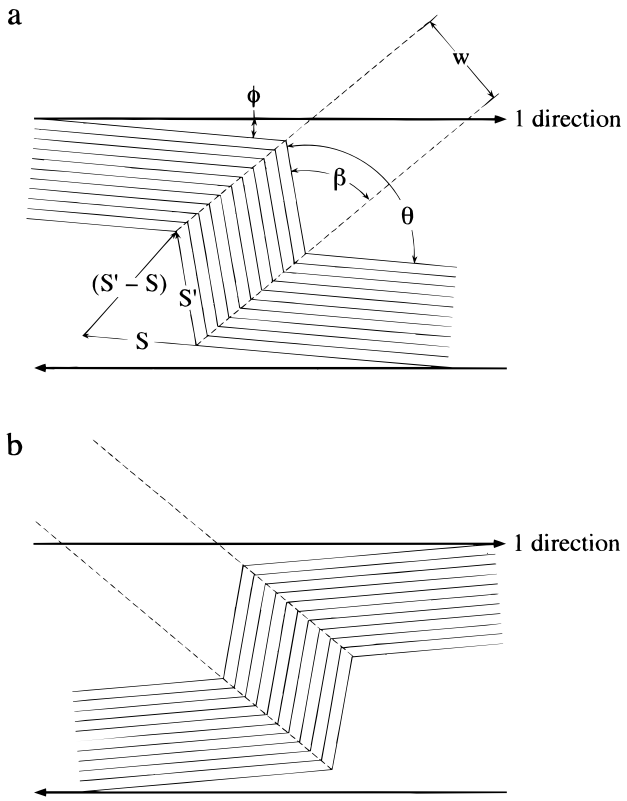

Figure 4. Schematic representation of (a) a forward kink band and (b) a reverse kink band. The distinguishing feature between forward and reverse kink bands are their orientation relative to the shearing direction, which is represented by the bold arrows above and below the kink bands. The boundaries, indicated by dotted lines, of forward kink bands make acute angles with the shearing direction, whereas boundaries of reverse kink bands make obtuse angles with the shearing direction. The parameters used to describe the kink band geometry are shown in Figure 4a: the orientation of the kink band boundary relative to the lamellae inside the kink band (β), the orientation of lamellae in the matrix relative to the lamellae inside the kink band (θ), the orientation of lamellae in the matrix relative to the shearing direction (ϕ), and the kink band width (w). The boundary displacement, $|S' - S|$, is determined by combining β, θ, and w, assuming that the limb length remains constant throughout kink band formation ($|S'| = |S|$) and rotates through an angle ($180° - \theta$).

Figure 1b shows an SEM micrograph of an isolated kink band following steady shear at 0.05 s^{-1} and a strain of 80%. The orientation of the steady shear relative to the image plane is shown in the inset of Figure 1b, and is the same for all the micrographs in this paper. The forward kink bands produced by steady shear have the same characteristics as kink bands in other layered materials: two rows of oppositely sensed angular hinges separating the lamellae inside and outside the band. A forward kink band forms an acute angle between the kink band boundary and the velocity direction. Forward and reverse kink bands are shown schematically in Figures 4 a and b, respectively. Steady shear produces only forward kink bands, whereas oscillatory shear can produce conjugate kink bands (conjugate kink bands consist of two sets of forward kink bands, one set produced during the forward motion and the second set produced during the reverse motion in oscillatory shear).[12]

Kink bands similar to that just described form at steady shear rates between 0.005 and 0.1 s^{-1}, but only at shear strains above a critical strain. Figure 5 shows the morphologies for samples sheared at 0.05 s^{-1} in

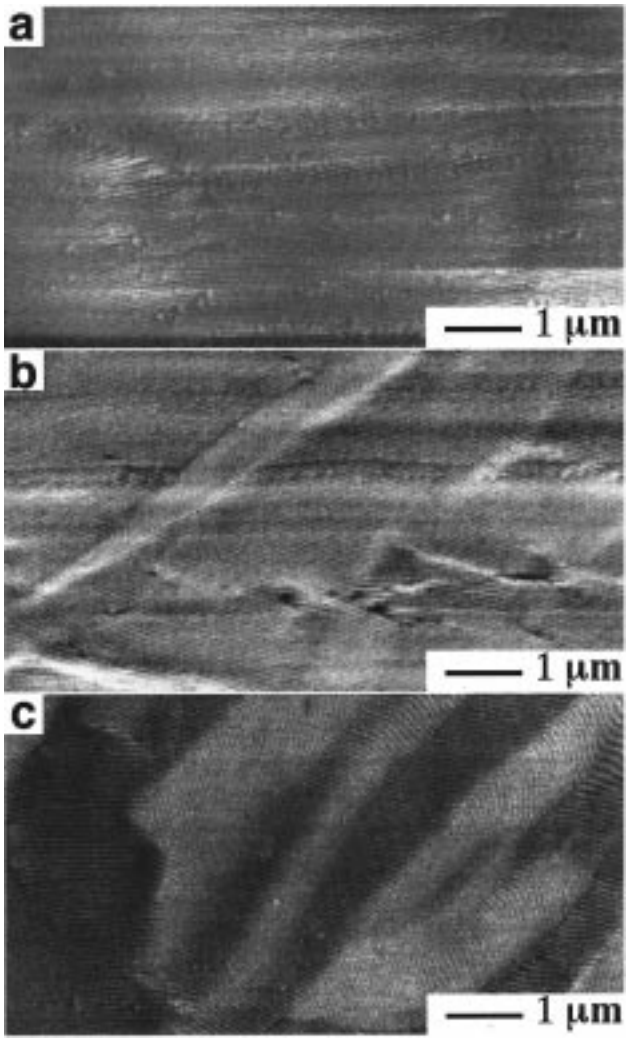

Figure 5. FE-SEM micrographs of SEP(40−70) following alignment and steady shear at 180 °C, 0.05 s^{-1}, and (a) 20% strain, (b) 40% strain, and (c) 80% strain. No kink bands result from 20% strain. Shear strains of 40 and 80% produce kink bands that increase in number density with additional strain. The orientation of the steady shear is as shown in the inset of Figure 1b.

which 20% strain does not produce kink bands, whereas shear strains of 40 and 80% do produce kink bands. At this rate, as well as at 0.005 and 0.1 s^{-1}, the critical strain is between 20 and 40% for SEP(40−70) at 180 °C. The shear rates studied are much faster than the estimated time for junction points to diffuse along the interface (described by Rubinstein and Obukhov as lamellae "melting"[13]), and therefore may explain why the critical strains are similar for the range of rates tested. Above the critical strain, there is apparently no systematic variation in kink band geometry with strain. However, there is an increase in the number density of kink bands with increasing strain (Figures 5 b and c). At this point, our experiments cannot distinguish between critical strain and critical stress.

To further examine kink initiation, samples were strained 30% (Figure 6). No kink bands were observed; however, rounded S-folds that are probably precursors to kink bands were observed. These S-folds have many of the same characteristics as kink bands: forward orientation relative to the shearing direction, opposite sensed boundaries, and widths on the order of 0.5 μm. The main distinguishing feature is the sharpness of the

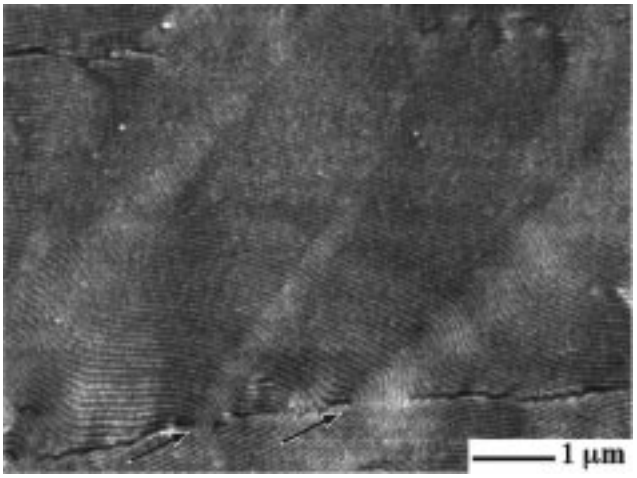

Figure 6. FE-SEM micrographs of SEP(40−70) following alignment and steady shear at 180 °C, 0.005 s^{-1}, and 30% strain. No kink bands result; however, rounded *S*-folds are observed. These *S*-folds are similar to kink bands in that they have similar orientation relative to the shearing direction, opposite sensed boundaries, and widths of ~0.5 μm. They differ only in the sharpness of the boundaries, where kink band boundaries have radii of curvature on the order of 50 nm and *S*-folds have radii of curvature on the order of 250 nm. These *S*-folds are often observed initiating at defects, as indicated by the arrows. The orientation of the steady shear is as shown in the inset of Figure 1b.

boundaries, where kink band boundaries have radii of curvature (R_c) that are typically less than the layer periodicity (D).[14] We observe $R_c \sim 50$ and 250 nm for kink band boundaries and S-fold boundaries, respectively, as compared with $D_{eq} \sim 72$ nm.[11] The rounded folds typically emanate from defects such as those marked by arrows in Figure 6. These defects produce local variations in lamellar orientation that may be enhanced by steady shear, leading to kink bands.

Throughout the remainder of this work we characterize kink bands near the center of the bands where the boundaries are nearly parallel and the geometry can be defined by three parameters: kink band width (w), the angle between the kink band boundary and the lamellae inside the kink band (β), and the angle between lamellae outside and inside the kink band (θ); see Figure 4a. An additional angle, ϕ, is required to describe the orientation of a kink band relative to the shearing direction. This angle can be thought of as the misalignment of the matrix lamellae (lamellae near but outside a kink band) relative to the shearing direction. We determined w, β, θ, and ϕ from scanning electron micrographs for a number of kink bands at each shearing condition above the critical strain. For each kink band, w, β, θ, and ϕ are calculated as an average from three locations along the central region of the kink band. In the case of the kink angles, we incorporate measurements from both upper and lower boundaries into the average (i.e., an average of six measurements). The angles measured from the two boundaries are not systematically different and therefore justify this type of averaging. In the remainder of this paper, range and average values refer to measurements from multiple kink bands at particular shearing conditions as opposed to the range and average values from a single kink band.

The kink band width, w, exhibits a range of ~ 0.2−1.0 μm and an average of ~ 0.6 μm at each shearing condition in this study, suggesting that it is independent of both strain and strain rate. Moreover, no correlation

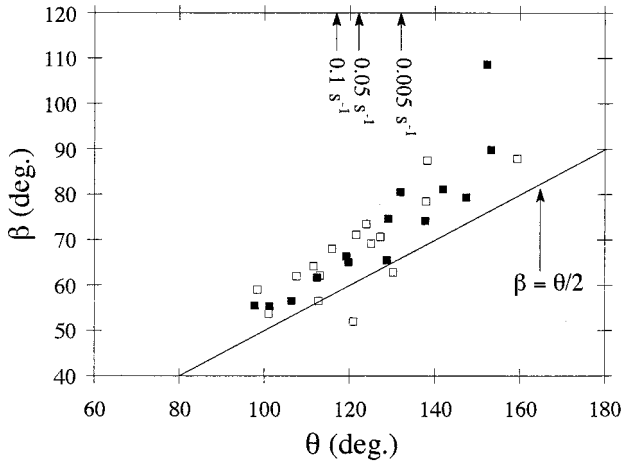

Figure 7. Plot of β versus θ for kink bands produced in samples strained 40% (filled squares) and 80% (open squares). The range of β ($\sim$ 50−90°) and θ ($\sim$ 95−160°) are similar for both strains. No distinction is made between rate, although the average θ for each rate is indicated by arrows at the top of the plot. The average θ decreases with increasing rate. The solid line represents the condition $\beta = \theta/2$, showing that the majority of kink bands have $\beta > \theta/2$. This result indicates a dilation of the lamellae inside the kink band relative to lamellae in the neighboring matrix.

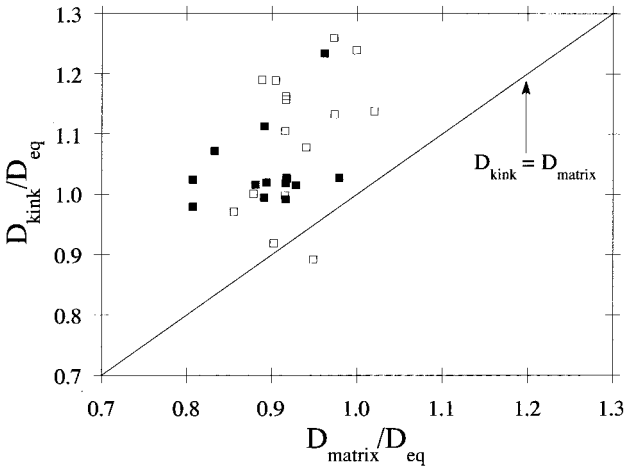

Figure 8. Plot of D_{kink}/D_{eq} versus D_{matrix}/D_{eq} for kink bands produced in samples strained 40% (filled squares) and 80% (open squares). The solid line indicates the condition that $D_{kink} = D_{matrix}$. Consistent with Figure 7, points above the solid line indicate a dilation of lamellae in the kink bands relative to the matrix. Furthermore, the majority of kink bands have $D_{kink} > D_{eq} > D_{matrix}$, which is the case in the upper left quadrant of the plot. D_{eq} is the equilibrium lamellar long period (71.5 ± 0.3 nm[11]).

was found between w and rate based on a nonparametric analysis ($r = 0.057$ and $p = 0.7651$, where r represents Spearman's rank correlation coefficient and p corresponds to the significance level of a statistical null hypothesis test that $r = 0$[15]). Additionally, a range of kink angles are observed for each shearing condition. Figure 7 shows β versus θ for kink bands in samples strained 40 and 80%. The range of θ is similar ($\sim$95−160°) for both 40 and 80% strain. Figure 7 does not differentiate kink band geometry based on shear rate, however, the average θ for each rate is marked by an arrow. Although shear rates of 0.005, 0.05, and 0.1 s^{-1} show similar ranges for kink band angles, the average θ decreases with increasing rate. That is to say, faster shearing leads to kinked lamellae that are closer to the transverse orientation ($\theta = 90°$). However, the correlation between θ and rate is weak ($r = -0.374$ and $p = 0.0418$), and additional data are needed to make a conclusive statement regarding the rate dependence. The orientation of the kink boundary relative to the 1-direction is calculated using the angles already described ($\theta-\beta-\phi$). The average boundary orientation decreases slightly with increasing strain rate, from 48° at 0.005 s^{-1} to 41° at 0.1 s^{-1}. This decrease does not appear to be a result of the misalignment (ϕ) based on the fact that ϕ and rate are not correlated ($r = -0.059$ and $p = 0.7559$).

The strongest correlation, as expected due to lamellar continuity through the tilt walls, is between β and θ, ($r = 0.886$ and $p = 0.0001$). The solid line in Figure 7 represents the condition $\beta = \theta/2$, corresponding to lamellae inside and outside the kink band with the same lamellar long period ($D_{kink} = D_{matrix}$). We observe $\beta > \theta/2$ for the majority (> 90%) of kink bands. This result indicates a dilation of the lamellae inside the kink bands relative to the lamellae in the matrix (close to the kink band; $D_{kink} > D_{matrix}$). Figure 8 shows a plot of (D_{kink}/D_{eq}) versus (D_{matrix}/D_{eq}) measured from Fourier transforms of the SEM micrographs for both 40 and 80% strain. The parameter D_{eq} is the equilibrium lamellar long period, 71.5 ± 0.3 nm, determined from SAXS.[11]

Consistent with the β, θ data, the majority of kink bands show a dilation of the lamellae within the kink bands relative to the lamellae outside the kink bands; that is (D_{kink}/D_{eq}) > (D_{matrix}/D_{eq}). Furthermore, the majority of kink bands have $D_{kink} > D_{eq} > D_{matrix}$, which is the condition in the upper left quadrant of Figure 8. Note that a contraction of the matrix lamellae following oscillatory shear was previously reported by Pinheiro et al.,[11] consistent with predictions of Williams and MacKintosh.[16]

To compare the strain localization in the kink bands, β, θ, and w from the center of a kink band are combined to estimate the average boundary displacement. This method is based on a fixed hinge model developed by Peacock[17] to describe kink band boundary displacement as a function of distance along the boundary. Peacock's hinge model estimates the average displacement at the boundary ($|S' - S|$) by assuming that the limb length remains constant ($|S| = |S'|$) and rotates through an angle of ($180° - \theta$) to its final, observed position (Figure 4a). The value $|S' - S|$ is given in terms of the measured kink band parameters as follows:

$$|S' - S| = \frac{w}{\sin\beta}\sqrt{2 - 2\cos(180° - \theta)} \qquad (1)$$

At each shear rate, a range of local displacements, $\sim$ 0.13−1.3 μm, exists as expected for a defect morphology. Moreover, the range of $|S' - S|$ is similar for 40 and 80% strain, suggesting that additional applied strain is accommodated by initiating more kink bands. This result is consistent with the observed increase in the number density of kink bands with increasing strain, as shown in Figures 5 b and c. Note that calculating $|S' - S|$ by assuming a constant kink volume, which allows the limb length to shorten due to $D_{kink} > D_{matrix}$ rather than a constant limb length, does not significantly alter the results.

Okamoto et al.[18] and Pinheiro et al.[11] found that LAOS can stabilize lamellae in the transverse orientation in PS−PEP samples, creating a parallel-transverse biaxial texture from specimens that were unaligned.

Further morphological studies revealed that these shear-stabilized structures were conjugate kink bands,[12] suggesting that kink bands are stable in forward/reverse shear fields. In contrast, Zhang and Wiesner[19] and Z.-R. Chen and co-workers[20] observed transient biaxial orientations during LAOS ($\omega \gg \omega'_c$) in lower molecular weight poly(styrene-*b*-isoprene) lamellar diblock copolymers. These discrepancies may be due to the details of the material properties and/or differences in the starting states, which we address in the following section. Here, we examine the stability of forward kink bands subjected to reverse half cycles of shear; that is, negative steady shear. An initially aligned SEP(40−70) specimen was deformed by positive steady shear (0.1 s^{-1} to a strain of 40%) followed by negative steady shear (−0.1 s^{-1} to a strain of −40%). Examination of the morphology following this forward/reverse deformation showed no evidence of kink bands in the forward direction relative to the positive steady shear. However, forward kink bands relative to the negative steady shear were produced. That is to say, kink band boundaries were observed at ∼135° relative to the original or positive shearing direction, and not at ∼45°. Therefore, kink bands produced by steady shear in a SEP(40−70) specimen, with a predominately parallel initial orientation, are "erased" by steady shear in the opposite direction.

Discussion

In this section we discuss the preferential slip plane, mechanisms for kinking, and kink band stability. To evaluate the location of the preferential slip plane in this diblock copolymer we estimate the stiffness of the PS and PEP microdomains and compare the number of entanglements between opposing blocks. Although we cannot observe kink band formation in situ, we compare our results regarding kink band geometry to those expected for two contrasting models, fixed hinge-rotation and boundary migration. This comparison provides insight into the mechanism of kink band formation and is presented in the general context of folding phenomena, which includes chevron folds. Finally, we examine how varying the starting state alignment can affect the stability of kink bands produced by oscillatory shear.

The formation of kink bands in SEP(40−70) implies the presence of a preferential slip plane parallel to the lamellar microdomains.[3] In the case of foliated rocks, such as the laminated siltstone/clay multilayer shown in Figure 1a, shear strain occurs preferentially in the less competent clay-rich layers that are macroscopic in thickness.[4] In minerals and other crystalline solids, the preferential slip occurs in an analogous manner, but on a finer size scale between crystallographic planes. In a diblock copolymer, slippage is unlikely to occur at the intermaterial dividing surface between the microdomains because the molecules are covalently bonded across the interface. Rather, the preferential shear deformation must be within one or both of the lamellar microdomains. To compare the stiffness of the PS and PEP lamellae, we estimate the zero shear viscosity (η_o) for homopolymers of equivalent molecular weight (M) to the blocks of the copolymer. This estimate is based on the uncorrelated drag model of Graessley:[21]

$$\eta_o \cong \frac{0.0027\rho N_{av} a^2 \zeta_o M^{3.5}}{M_e^{2.5} M_o^2} \qquad (2)$$

where ρ is polymer density, N_{av} is Avogadro's number, a is the Kuhn length, ζ_o is the monomeric fiction coefficient, M_e is the entanglement molecular weight, and M_o is the molecular weight per monomer unit. The monomeric friction coefficient, ζ_o, at 180 °C was extrapolated from data reported in ref 21 assuming Williams−Landel−Ferry (WLF) behavior for PS and Arrhenius behavior for PEP to give 5.2e-7 and 1.3e-9 dynes s cm^{-1}, respectively. However, the entanglement molecular weights for PS and PEP are 17 300 and 1660 g/mol, respectively, which compensates for the difference in ζ_o in the calculations of η_o.[21] Thus, at 180 °C, η_o for 40 000 g/mol PS and 70 000 g/mol PEP are ∼140 and ∼850 dynes s cm^{-2}, respectively, indicating a slight preference for deformation in the PS microdomains.

The estimate just presented assumes the microdomains deform similarly to their entangled homopolymer equivalents. However, the microdomains are more comparable to opposing grafted polymer brushes, in which one end is confined to the intermaterial dividing surface and the entanglement density varies normal to the lamellae. Therefore, the shear deformation could be localized in the regions of interpenetration between opposing PS or PEP blocks or brushes.[13,22,23] A Witten-Pincus-Leibler model predicts the interpenetration thickness between these opposing brushes to be ∼4.5 and ∼6.0 nm for the PS and PEP lamellae, respectively.[22] These thicknesses correspond to molecular weights of ∼14 000 and ∼21 000 g/mol in the interpenetration zones of the PS and PEP lamellae, respectively. This analysis suggests that the PEP blocks are significantly entangled across the lamellae whereas the PS blocks are comparatively unentangled. Consequently, the PS microdomains may relax according to Rouse dynamics because they are unentangled with the opposing brushes. On the other hand, the PEP brushes, which are well entangled with opposing brushes, may undergo an arm retraction type relaxation. This mechanism is similar to that of star polymers, where the relaxation time depends exponentially on the number of entanglements per chain. Furthermore, Rubinstein and Obukhov[13] predict that the relaxation times for the interpenetrating brushes could be considerably longer due to fluctuations in the number of entanglements per chain.

Although estimates of the zero shear viscosities do not clearly indicate a preferential slip plane, analysis of the interpenetration zones suggests that the PS microdomains can deform more easily than the PEP microdomains. A preferential slip plane is necessary for kink band formation, and this analysis suggest that such a slip plane exists in the PS microdomains of this lamellar diblock copolymer at 180 °C. This result is contrary to what a simple inspection of the block T_gs would indicate. It is important to distinguish between slip in the PS, PEP, or both microdomains, even though all three situations could lead to kinking. If slip occurs in both lamellae, then one might expect that the junction points could diffuse along the intermaterial dividing surface. The relaxations in this case differ from the case of slip in one domain with the junction points nearly fixed. Furthermore, for quantitative purposes and potential theoretical descriptions or simulations of the phenomena, it is important to know the degree of strain localization that would lead to a different threshold criteria for kinking.

Two models have been proposed in the field of structural geology for kink band formation, fixed hinge-

rotation and boundary migration.[3,14] The fixed hinge model suggests that the limb length, $|S|$, is established at small strains and remains constant as the limbs rotate through an angle $(180 - \theta)$ during kink band formation. In this case, the boundaries have a fixed orientation relative to the shearing direction throughout kink band growth while the layers inside the bands rotate. This leads to variations in layer separation during rotation. At some final rotation angle, the fixed hinge mechanism is exhausted and additional strain is accommodated by the initiation of new kinks and/or by other mechanisms. In contrast, the boundary migration model suggests that kink bands nucleate as points or lines. The boundaries, with fixed orientation relative to the shearing direction, migrate both laterally and longitudinally into unkinked material with additional strain. In the boundary migration model, the kink angles, θ and β, remain constant throughout the growth process, moreover, the kink bands remains symmetric during growth (i.e., $\beta = \theta/2$). Although both mechanisms involve reorientation of the lamellae, the rotation is localized at the tilt boundaries in the boundary migration model.

Our observations regarding kink band formation in SEP(40−70) are more consistent with a fixed hinge mechanism. We observe similar ranges and average kink band widths for each shearing condition, indicating that there is no strain or strain rate dependence on width. This result suggests that kink band width is set by some type of instability as in the case of the fixed hinge model. In contrast, the boundary migration model predicts that the width should vary with strain. A range of kink angles (β and θ) at each shearing condition above the critical strain is also consistent with limb rotation, as in the fixed hinge model. The range of kink band angles at a particular strain and strain rate could be the result of variations in initial orientation and/or time since kink initiation. Furthermore, we observe asymmetric kink bands ($\beta > \theta/2$) associated with a lamellar dilation in the kink bands, which is expected for a fixed hinge growth process. The boundary migration model predicts that β and θ are fixed during kink band growth and that $\beta = \theta/2$, contrary to our observations. Although additional experiments are needed to conclusively determine the mechanism of kink formation in block copolymers, strain-independent kink band widths, a range of kink band angles at each shearing condition, and asymmetric kink bands all suggest a fixed hinge-rotation mechanism.

In other studies, lamellar[5] and cylindrical[6] block copolymers have been reported to form chevron folds, an alternative fold morphology that is also widely reported in geology. We propose that kink folds and chevron folds are both manifestations of the same deformation mechanism; that is, layer slip and limb rotation. One of the factors effecting the selection of kink folding versus chevron folding is the orientation of the principle stresses relative to the foliation. For the observation of chevron folding by Hudson and coworkers,[5] the maximum extension, σ_1, was oriented normal to the lamellae. They found that tilt walls were produced parallel to σ_1.[5] Figure 9a shows schematically how chevron folds could develop, where tilt walls or strain invariant planes form parallel to σ_1 and rotation of lamellae occurs via opposing layer slip on either side of these walls, to produce periodic, angular folds. This type of folding may be preceded by a periodic instability,

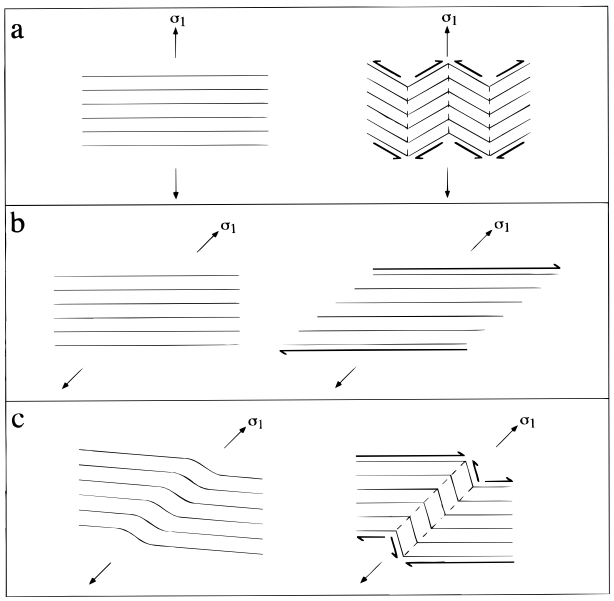

Figure 9. Schematic illustrating possible mechanisms for chevron fold and kink band formation. (a) When the direction of maximum extension, σ_1, is oriented normal to the lamellae, chevron folds develop by opposing lamellar slip about tilt walls oriented parallel to σ_1. (b) When σ_1 is oriented at 45° relative to the lamellae, uniform layer sliding occurs without rotation of the lamellae. (c) If local misorientations perturb the situation described in (b), such that shear stresses parallel to the slip plane vary along the lamellae, then kink bands form. This illustrates the similarities between chevron fold and kink band formation, whereby tilt walls are produced parallel to σ_1 and opposing lamellar slip occurs about these tilt walls. However, chevron folds differ from kink bands in that they are periodic folds and are symmetric about the tilt walls.

such as low-amplitude sinusoidal folding, a buckling type instability.[24] Alternatively, if the direction of maximum extension is oriented at 45° to the lamellar normals (i.e., shearing parallel to the layers), then sliding of lamellae can occur uniformly without rotation (Figure 9b). However, an instability that causes nonuniform lamellar sliding could lead to kink band formation by a similar mechanism to that already described; that is, opposing limb rotation. One source of a discrete instability is a preexisting defect that causes local misorientation of lamellae, such that the shear stresses vary along the lamellae, as shown in Figure 9c. Other possible sources of instabilities include stick-slip within microdomains[23] and buckling of the lamellae. Chevron folds differs from kink bands in that the structure is periodic and the limbs are symmetric about the tilt walls. However, both chevron folds and kink bands may form by a similar mechanism, in which strain invariant planes form parallel to the direction of maximum extension and opposing lamellar slip occurs on either side of these planes.

Our observations suggest that residual defects in the predominately parallel starting state nucleate kink bands. We find clustering of both residual defects and kink bands that support this relationship. The kink band widths also have the same characteristic size (∼0.5 μm) as residual defects in the initially aligned specimens. At 30% strain (Figure 6) we observe rounded folds emanating from defects. At 40 and 80% strain we often observe kink bands emanating from defects. These rounded folds are similar to kink bands in all respects except boundary curvature and may be precursors to kink bands. Because the defects differ slightly

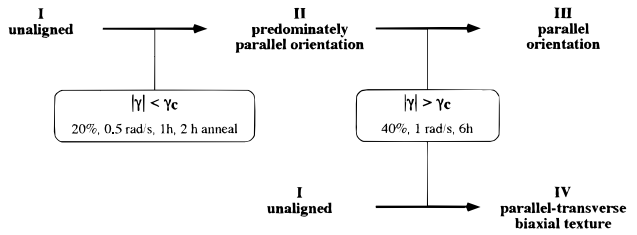

Figure 10. Schematic showing two orientation pathways. A parallel orientation can be produced from an initially unaligned SEP(40−70) specimen (**I**) in two steps. First, applying LAOS with a strain amplitude below the critical strain required to produce kink bands, $|\gamma| < \gamma_c$, leads to a predominately parallel orientation (**II**). After this initial alignment, applying LAOS with $|\gamma| > \gamma_c$ leads to a parallel orientation (**III**), because kink bands are not stable relative to reverse cycles of shear in a predominately parallel orientation. In contrast, if the same conditions of LAOS that were used to go from **II** to **III** (i.e., $|\gamma| > \gamma_c$) are used on **I**, then a parallel-transverse biaxial orientation (**IV**) results. This result suggests that the stability of kink bands depends on the overall alignment and/or defect density of the specimen.

in size and curvature, they could produce different initial limb lengths and orientations, leading to a strain-independent range of kink band widths and angles at each shearing condition above the critical strain, as observed. Furthermore, the critical strain may be associated with the deformation required to sharpen the rounded boundaries near defects.

We have found that a critical strain is required to produce forward kink bands in SEP(40−70) with steady shear. Furthermore, reverse steady shear "erases" these forward kink bands. We have applied these results to LAOS, allowing us to better control the morphology of SEP(40−70), a high molecular weight, well segregated block copolymer. Figure 10 schematically shows orientation pathways leading to a parallel orientation (III) and a parallel-transverse biaxial orientation (IV). Consider a SEP(40−70) specimen that is initially unaligned, with a weak preference of the parallel orientation (I). Applying LAOS to this unaligned specimen (I) with a strain amplitude less than the critical strain, $|\gamma| < \gamma_c$, does not produce kink bands and the predominately parallel orientation (II) is induced. From our steady shear studies we know that kink bands are not stable relative to reverse half cycles of shear in an initially aligned (predominately parallel) specimen. Therefore, applying LAOS with $|\gamma| > \gamma_c$ to a predominately parallel orientation (II) forms and destroys forward kink bands, resulting in an enhanced parallel orientation (III). In contrast, applying LAOS, $|\gamma| > \gamma_c$, to the unaligned specimen (I) produces conjugate kink bands, resulting in the parallel-transverse biaxial orientation (IV). The conjugate kink bands are produced because $|\gamma| > \gamma_c$, and these forward kink bands, which are produced in both directions, persist during reverse cycles of shear in this initially unaligned material. Figure 11 shows $I_4(\mu)$ as a function of μ, from 2-D SAXS patterns in the 1*-2* plane, for specimen I, II, III, and IV. Because a critical strain is required to produce kink bands and kink bands in a predominately parallel orientation are not stable relative to reverse cycles of shear, "strain ramping" can be used to produce well-aligned parallel SEP(40−70) specimens. The reason for kink band stabilization in an unaligned specimen is unclear. One possibility may be that the stability of kink bands depends on the overall alignment and/or defect density of the specimen. If a reverse cycle of shear requires significant matrix slip to erase a kink band, neighboring kink bands and other defects could hinder the relaxation and thereby stabilize the kink bands.

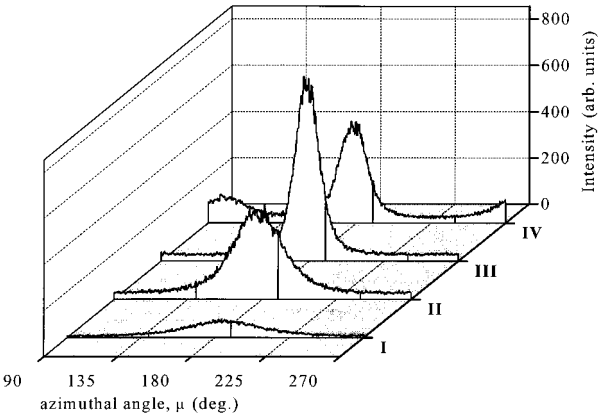

Figure 11. $I_4(\mu)$ as a function of μ for SEP(40−70) specimens **I**, **II**, **III**, and **IV**, which are described in Figure 10. All the intensity distributions correspond to SAXS experiments in which the beam was orientated parallel to the 3* direction, such that 90° and 270° correspond to the 1* direction and 180° corresponds to the 2* direction. Specimen **I** shows a slight preference of the parallel orientation due to solvent casting and compression molding, as indicated by the weak maximum at 180°. Specimen **II** shows a predominately parallel orientation as described in more detail in Figure 2. Specimen **III** shows an enhancement of the parallel orientation relative to **II**, exhibiting a more intense and narrower maximum centered at 180°. Specimen **III** shows no signs of a biaxial orientation, which is evident from the uniform scattering intensity at ≈90° and 270°. In contrast, **IV** shows maxima at both ∼90° and 180° corresponding to a parallel-transverse biaxial orientation.

Conclusion

Above a critical strain, steady shear induces forward kink bands in initially aligned SEP(40−70) specimens. Kink band formation in this block copolymer is consistent with a fixed hinge-rotation mechanism. These results provide evidence for the existence of a preferential slip plane and rotation of lamellae during deformation. We determined that preferential slip occurs in the PS microdomains due to fewer entanglements between opposing brushes. We propose that kink bands form by opposing slip along the lamellae about strain invariant tilt walls. This mechanism may also be responsible for previously observed chevron folding. Our results also suggest that existing defects play an important role in both kink band initiation and stabilization. Lowering the defect density prevents kink band stabilization, as was demonstrated in a comparison between two different LAOS pathways. Specifically, strain ramping can be used to avoid previously reported biaxial orientations and produce a well-aligned morphology in this high molecular weight, well segregated block copolymer.

Block copolymer dynamics and morphological development have received considerable attention from researchers over the past two decades, yet many of the important issues remain unresolved. We have taken a new approach in studying this problem, namely, to create and control specific defects. Although additional work is necessary to extract materials parameters from kink band studies, this work demonstrates the importance of defect-mediated rheology in block copolymers.

Acknowledgment. Work at the University of Pennsylvania was supported by NSF-DMR-MRSEC (9632598), NSF-DMR-YIA (9457997), and Procter & Gamble. Special thanks to Adam Polis, Senior Statistician, Merck & Company, Inc., for his help with the statistical analysis and Robert Armitage for his assistance with SAXS experiments. The authors also thank Prof. John Bassani, Dr. Alex Levine, Dr. Scott Milner, and Prof. David Morse for helpful discussions.

References and Notes

(1) Orowan, E. *Nature* **1942**, *149*, 643.
(2) Voll, G. *Liv. Manch. Geol. J.* **1960**, *2*, 503.
(3) Anderson, T. B. In *The Encyclopedia of Structural Geology and Plate Tectonics*; C. K. Seyfert, Ed.; Van Nostrand Reinhold: New York, 1987; Vol. 10; p 373.
(4) Ramsay, J. G.; Huber, M. I. *The Techniques of Modern Structural Geology: Folds and Fractures*; Academic: London, 1987; Vol. 2, p 700.
(5) Hudson, S. D.; Amundson, K. R.; Jeon, H. G.; Smith, S. D. *MRS Bull.* **1995**, *20*, 42.
(6) Honeker, C. C.; Thomas, E. L. *Chem. Mater.* **1996**, *8*, 1702.
(7) Colby, R. H. *Curr. Opin. Coll. Interface Sci.* **1996**, *1*, 454.
(8) Fredrickson, G. H.; Bates, F. S. *Annu. Rev. Mater. Sci.* **1996**, *26*, 501.
(9) Chen, Z.-R.; Kornfield, J. A.; Smith, S. D.; Grothaus, J. T.; Satkowski, M. M. *Science* **1997**, *277*, 1248.
(10) Csernica, J.; Baddour, R. F.; Cohen, R. E. *Macromolecules* **1987**, *20*, 2468.
(11) Pinheiro, B. S.; Winey, K. I.; Hajduk, D. A.; Gruner, S. M. *Macromolecules* **1996**, *29*, 1482.
(12) Polis, D. L.; Winey, K. I. *Macromolecules* **1996**, *29*, 8180.
(13) Rubinstein, M.; Obukhov, S. P. *Macromolecules* **1993**, *26*, 1740.
(14) Weiss, L. E. *Tectonophysics* **1980**, *65*, 1.
(15) A rank correlation test examines whether a monotonic relationship exists between two variables (x, y). Because this type of test examines the ranks of the data rather than the actual observed data it does not assume any distribution and is not significantly affected by outliers. Specifically, Spearman's rank correlation coefficient, r, is calculated using Pearson's formula applied to the ranks. The values of r ranges from -1 to 1, where $r < 0$ correspond to a monotonic decrease (if $x_2 > x_1$, then $y_2 \leq y_1$) and $r > 0$ correspond to a monotonic increase (if $x_2 > x_1$, then $y_2 \geq y_1$). The p value corresponds to the fraction of the permutations of ranks with an r more extreme than the determined r (i.e., p is the probability that the r value was determined by chance).
(16) Williams, D. R. M.; MacKintosh, F. C. *Macromolecules* **1994**, *27*, 7677.
(17) Peacock, D. C. P. *Tectonophysics* **1993**, *220*, 13.
(18) Okamoto, S.; Saijo, K.; Hashimoto, T. *Macromolecules* **1994**, *27*, 5547.
(19) Zhang, Y.; Wiesner, U. *J. Chem. Phys.* **1995**, *103*, 4784.
(20) Chen, Z.-R.; Issaian, A. M.; Kornfield, J. A.; Smith, S. D.; Grothaus, J. T.; Satkowski, M. M. *Macromolecules* **1997**, *30*, 7096.
(21) Ferry, J. D. *Viscoelastic Properties of Polymers;* third ed.; John Wiley & Sons: New York, 1980.
(22) Witten, T. A.; Leibler, L.; Pincus, P. A. *Macromolecules* **1990**, *23*, 824.
(23) Joanny, J. F. *Langmuir* **1992**, *8*, 989.
(24) Johnson, A. M. *Styles of Folding;* 1st ed.; Elsevier Scientific Publishing: New York, 1977; Vol. 11, p 406.

MA971839A